IV.2. IRON FISCHER-TROPSCH CATALYSTS. STRUCTURAL FEATURES IN THE FORMATION OF THE GREEN RUST INTERMEDIATE AND γ-FeOOH. (Ram Srinivasan, Rongguang Lin, Robert L. Spicer, and Burtron H. Davis

IV.2.1. ABSTRACT

Electron microscopy data reveal a pattern of changes in the particle shape/morphology during the preparation of γ-FeOOH. The initial shapeless material develops to form large thin hexagonal crystals which are shown to be Green Rust-II (GR-II). With the initial, sudden pH decrease from about 8 to 6.5 at about 33% conversion of the total amount of Fe^{2+} that is oxidized, small, dense, hexagonal Fe_3O_4 particles are formed in addition to, or instead of, the GR-II hexagonal crystals. The large thin hexagonal crystals of Gr-II contain holes. The disappearance with further oxidation of Fe_3O_4 and GR-II particles is accompanied by the development of needle-type γ-FeOOH particles. The formation of γ-FeOOH by a pathway involving only GR-II is therefore an oversimplification of the actual process.

IV.2.2. INTRODUCTION

The formation of uniform colloidal particles involves many factors. For example, in precipitation reactions involving inorganic salts, the type of precursor may influence the structure and properties of the end-products and one or more solute complexes may be involved. Many hydrated polyvalent metal ions have the tendency to deprotonate in aqueous solutions at elevated temperatures and this approach has been utilized in attempts to achieve the formation of uniform particles. However, other factors, such as the pH, the nature and the concentrations of anions, the temperature,

drying conditions, etc., may play dominant roles in the evolution of the shape and structure of the final product.

The study of ferrous (Fe^{2+}) and ferric (Fe^{3+}) ions has drawn considerable attention, as the iron system finds numerous applications in catalysis, ceramics, pigments, films, recording materials, coatings, corrosion science, etc. In corrosion, various forms of oxides, oxyhydroxides, and amorphous matter are believed to be the products that result from atmospheric corrosion (IV.2.1-IV.2.3), marine corrosion (IV.2.4), and passivation (IV.2.5). The formation and transformation mechanisms of iron oxides and oxyhydroxides have been investigated; these studies concentrated on the solid species, dissolved species, and their structural inter-relationships (for example, IV.2.6-IV.2.10). Studies on the mechanisms of formation of iron oxide and oxyhydroxides in aqueous solutions at room temperature were carried out by Misawa et al. (IV.2.11); these dealt with the formation mechanism of Fe_3O_4, α-FeOOH, β-FeOOH, γ-FeOOH, δ-FeOOH, amorphous ferric oxyhydroxide, and Green Rusts. It was claimed (IV.2.11) that the solid state transformation of $Fe(OH)_2$ to δ-FeOOH occurs upon oxidation with H_2O_2 in strongly alkaline solutions. However, in slightly alkaline solutions containing $Fe(OH)_2$, Green Rusts I or II (GR-I or GR-II) are formed as intermediate complexes as a result of solid state reaction during the slow oxidation of $Fe(OH)_2$.

The structure and composition of GR-I and GR-II are not well defined. GR-I has a dark green color as the name implies. Keller (IV.2.12,IV.2.13) described GR-I as a compound of composition between $4Fe(OH)_2 \bullet FeOCl$ and 2.17 $Fe(OH)_2$ 1.83 $FeOOH \bullet FeOCl$. Keller (IV.2.12) suggested varying compositions at different degrees

of oxidation, and assigned dimensions to the hexagonal unit cell of a_o = 3.22Å, c_o = 24Å if the precursor is a basic chloride, and a_o = 3.18Å, c_o = 22.96 ~ 22.25Å if the chloride is hydrated to an unstable double hydroxide $4Fe(OH)_2 \bullet FeOOH$, and a_o = 3.18Å, c_o = 24.37Å if the green complex is produced from a sulfate solution. GR-II has a hexagonal unit cell with a_o = 3.17Å and c_o = 10.9Å and is believed to consist of four closely-packed oxygen-hydroxyl layers in an ABAC sequence (IV.2.6). It has been proposed that GR-II has a slightly dull dark green color with a composition of $4Fe(OH)_2 \bullet 2FeOOH \bullet FeSO_4 \bullet XH_2O$ (IV.2.14).

The objective of this investigation was to follow the structural and morphological changes that occur from the initial precipitation from an iron sulfate suspension to the formation of the final product of γ-FeOOH. These structural and morphological changes were followed using X-ray diffraction, transmission electron microscopy (TEM), and electron microdiffraction techniques. These studies on the oxidation of Fe(II) were carried out in concentrated solutions suitable of the peparation of iron catalyst, pigments, etc.

IV.2.3. EXPERIMENTAL METHODS

A ferrous sulfate solution (0.22M) was mixed in the absence of oxygen with the required amount of NaOH to produce a pH of 8.2 at 23°C. The ratio (R) of Fe^{2+} to OH^- was 7:12 (0.583). Argon was passed through a 5-neck round-bottom flask containing about 1.65 ℓ of ferrous sulfate solution for 1 hour to ensure that the $FeSO_4$ solution and the flask do not contain oxygen. A pH electrode, oxygen inlet line fitted with a fritted-glass bubbler, a mechanical stirrer, an oxygen outlet line, and a thermometer to monitor the temperature of the suspension were fitted into the five

openings of the flask. After a known amount of NaOH granules to produce a ratio (R) of 0.583 was added to the $FeSO_4$ solution, the suspension was stirred at 500 rpm. The pH of the suspension was monitored via the pH electrode. Following the precipitation of $Fe(OH)_2$ at a ratio of R = 0.583, the pH of the suspension was 8.2. As oxygen was bubbled through the suspension at a constant rate of 18.5 mL/min., the pH of the suspension remained almost constant at about 8.2 up to about 36 minutes. The variation in pH of the suspension with time is shown in Figure IV.2.1. At about 36 minutes the pH suddenly dropped to about 7.0; the pH then exhibited a slow decline with time up to 90 minutes when it abruptly dropped to about 4.0, and remained constant thereafter. As shown in Figure IV.2.1, the samples (L1 through L8) were withdrawn at different time intervals to follow the structural changes taking place along the pH-time curve. The specifications of the withdrawn samples are given in Table IV.2.1.

Each slurry sample (60 mL) was transferred by a syringe to a Schlenk filter tube which was flushed with ultra-pure nitrogen. The filter tube was sealed with a rubber septum. The solid was collected by filtration under a nitrogen atmosphere, washed two times with 50 mL of distilled water (free from oxygen), dried in vacuum at room temperature, and stored under a nitrogen atmosphere at 4°C to prevent oxidation.

Since the intermediate complexes (the so-called Green Rusts) are very sensitive to air oxidation, precautions were taken in preparing the samples for electron microscopy. Each sample was sealed in a glass vial in nitrogen. This vial was opened in a glovebox which was flushed with nitrogen. A small portion of the sample was transferred to a beaker containing degassed absolute ethanol and this

suspension was agitated in an ultrasonic bath which resulted in a suspension containing fine particles. A drop of this suspension was placed on a carbon coated 200 mesh copper grid. The ethanol evaporated, leaving a thin film containing particles of the iron species, and the grids were placed in a plastic vial which was immediately transferred to a vacuum desiccator to transport to the microscope room. Each sample was transferred from the desiccator and mounted into the microscope in less than 1 minute. Hence, all the samples were mounted for microscopic examination such that the maximum exposure to air, while transferring the grids to the TEM specimen holder, was less than 1 minute.

TEM examination was performed using a Hitachi H800 NA scanning transmission electron microscope at an operating voltage of 200 kV. Microdiffraction and EDX analyses were carried out in the nanoprobe (5 nm diameter) mode. This microscope is equipped with a silicon-lithium diode X-ray detector (Link Analytical Limited) and a multi-channel analyzer (Tracor 500). The X-rays emitted from the specimen upon electron irradiation were collected in the range 0.1 - 20 keV for 60 seconds.

X-ray diffraction was carried out using a Philips X-ray diffractometer outfitted with an XRG-3000 X-ray generator, and a graphite monochromator on the diffracted beam path. The data were collected using a VMS/VAX 700 system. The sample for XRD analysis was prepared in a glove box in a nitrogen environment. The sample was ground to a powder in an agate mortar and about one gram of the powder was pressed into the specimen holder in a nitrogen atmosphere. The sample was then quickly mounted into the diffractometer and the scan was carried out in air. The complete scan took less than 20 minutes.

IV.2.4. RESULTS

Samples were collected and characterized at several stages of precipitation (Figure IV.2.1). At each stage of sample withdrawal, the concentrations of Fe^{2+} and Fe^{3+} were determined by titration with a standard $KMnO_4$ solution. The molar fraction of Fe(II)/Fe(total) in the suspension linearly decreased with time and became constant at about 100 minutes (Figure IV.2.2). The added oxygen completely reacted with Fe(II) in the suspension; no oxygen was observed to evolve during the oxidation with an oxygen flow rate of 18.5 mL/min. After 100 minutes, the fraction of Fe(II) remained constant since the amount of NaOH added was not sufficient to precipitate all Fe(II), and the excess of Fe(II) ion was oxidized by oxygen very slowly in an acidic medium ($pH < 4$).

IV.2.4.a. L1 Sample

This sample was withdrawn after precipitation of $Fe(OH)_2$ but prior to initiating a flow of oxygen. A typical electron micrograph obtained from this sample (Figure IV.2.3) shows that there are regions consisting of thin, shapeless material, as well as the regions containing elongated, curly, dense particles. In addition, regions containing somewhat spherical particles in the size range of 10-30 nm are present; these are shown in Figure IV.2.4. This sample contains three notable regions, namely: (1) regions with thin, shapeless particles, (2) regions with thick, dense, elongated, curly particles, and (3) regions with spherical particles (a typical area for each region is identified in Figure IV.2.3). EDX data obtained from these regions showed only the presence of Fe; oxygen would not be detected with the instrument that was used. Using a 5 nm electron probe, several microdiffraction patterns were

obtained from typical areas of each of these regions. The shapeless, thin, transparent regions (region 1) are crystalline, and all such regions consistently exhibited ring diffraction patterns; a typical ring microdiffraction pattern is presented in Figure IV.2.5(a). Numerous crystalline sheets/particles in the shapeless region give rise to these ring patterns. Most commonly, ring patterns result from a large number of small grains (in this case, a large number of small particles) in the area illuminated by the beam. The rings actually consist of discrete beams from equivalent planes in each of the small particles. The ratio of the distance from the center to the first ring (R_1) and the second ring (R_2) is 0.562. Since the ratio R_1/R_2 is equivalent to the ratio of d_2/d_1, the [h,k,l] planes that yield the two rings can be obtained. The 'd' spacings for $Fe(OH)_2$ phase of [101] and [103] are 0.2403nm and 0.1349nm, respectively. The ratio of 'd' spacings of the [103] and [101] planes of $Fe(OH)_2$ is therefore 0.5614, and this is close to the experimental value of 0.5620 within a reasonable error of 0.11%. Also, the relative intensities of the [101] and [103] planes of $Fe(OH)_2$ are 100% and 60%, respectively, which are in agreement with the observed diffraction intensity. Hence, the first ring (d_1) and the second ring (d_2) probably correspond to the [101] and [103] planes of $Fe(OH)_2$, respectively. Incidentally, ferrous hydroxide ($Fe(OH)_2$) is a hexagonal close packed system with a_o = 0.3258nm and c_o = 0.4605nm. Several microdiffraction patterns obtained from similar shapeless transparent regions consistently yielded this type of ring patterns and therefore confirm that these regions are composed of large numbers of small particles of $Fe(OH)_2$. The electron microdiffraction pattern obtained from a thick spherical particle (Figure IV.2.4, region 3) is shown in Figure IV.2.5(b); this pattern corresponds to the $[100]_{hcp}$ orientation of

the $Fe(OH)_2$ phase. Several microdiffraction patterns obtained from other spherical particles consistently yielded the same spot diffraction patterns confirming the $[100]_{hcp}$ orientation of $Fe(OH)_2$. The curly dense elongated particles (region 2) were too thick to yield diffraction patterns.

The sample L1 consisted of three regions. While the shapeless, flat regions (region 1) yielded ring diffraction pattern of $Fe(OH)_2$, the spherical particles (region 3) showed diffraction spots corresponding to $Fe(OH)_2$ $[100]_{hcp}$ orientation. EDX patterns obtained from these regions showed only Fe. Based on these results, Sample L1 is confirmed to consist mostly, or completely, of crystalline $Fe(OH)_2$.

IV.2.4.b. L2 Sample

This sample was withdrawn after 13 minutes of oxidation, and the suspension corresponds to oxidation of 9% of the total Fe^{2+}. The micrographs obtained from this sample exhibits regions similar to those obtained for the L1 sample. Two typical electron micrographs obtained for this sample are presented in Figure IV.2.6(a) and IV.2.6(b) respectively. Electron microdiffraction data revealed that the transparent, shapeless regions are $Fe(OH)_2$ that produced ring diffraction patterns while the thick spherical particles showed diffraction patterns for $Fe(OH)_2$ (hcp phase). Hence, electron microscopy data show that L1 and L2, as far as the shape and morphology are concerned, are very similar.

IV.2.4.c. L3 Sample

This sample was collected after 37 minutes of oxidation at a stage where Green Rust should be present. The shape morphology for this sample differs significantly from the previous two samples. Large, thin, hexagonal crystals appear in this sample,

and these crystals contain many holes (Figure IV.2.7). The small holes in the size range from 2.5 - 3 nm are most prevalent in these crystals. However, holes as large as 12 - 14 nm in diameter were also observed, as shown in Figure IV.2.8. The average size of these thin hexagonal crystals is about 290 nm. Several microdiffraction patterns obtained from the thin hexagonal crystals consistently yielded orientations of GR-II crystals. A typical electron microdiffraction pattern obtained from a hexagonal crystal is presented in Figure IV.2.9(a) and the corresponding solution in Figure IV.2.9(b). EDX analysis from these thin crystals exhibited only FeK_{α} and FeK_{β} lines. It is surprising that lines corresponding to S were not observed. In addition to the formation of hexagonal crystals, evidence for the presence of γ-FeOOH fiber particles, and dense, elongated particles were obtained, as shown in Figure IV.2.10. The appearance of a very few thin fiber particles may be due to oxidation of green rust complexes while transferring the sample to the electron microscope. In any event, the large, thin crystals greatly outnumber the fiber particles.

X-ray diffraction pattern obtained for this sample exhibited peaks corresponding to GR-II structure.

IV.2.4.d. L4 Sample

This sample was withdrawn at a pH of about 6.75 after 48 minutes of oxidation. The X-ray diffraction pattern obtained from this sample is presented in Figure IV.2.11, and indicates the presence of two crystalline phases, namely, GR-II and Fe_3O_4. A representative electron micrograph for sample L4 is presented in Figure IV.2.12. Large, thin hexagonal crystals with small holes are still present. Also noticeably present are several dense hexagonal particles, which are in the size range of 20 - 70

nm. These dense hexagonal particles are consistently smaller than the large, thin hexagonal crystals (290 nm). In addition, fiber particles of γ-FeOOH are also evident in Figure IV.2.12. Several electron microdiffraction patterns were obtained from the dense hexagonal particles as well as from the large, thin hexagonal crystals. The diffraction patterns obtained from all the large, thin hexagonal crystals exhibited GR-II structure orientations. However, the microdiffraction patterns obtained from the smaller, dense hexagonal particles revealed the structure to be Fe_3O_4 (magnetite). Four most densely populated reciprocal lattice planes for the face-centered cubic Fe_3O_4 particles are given in Figure IV.2.13. Thus, the microdiffraction data indicating the presence of GR-II and Fe_3O_4 particles are in good agreement with the X-ray diffraction data shown in Figure IV.2.11. This sample consisted of predominantly large, thin hexagonal GR-II crystals, and smaller, dense hexagonal Fe_3O_4 particles.

IV.2.4.e. L5 Sample

This sample was withdrawn at a pH of 6.5 after 67 minutes of oxidation. A representative micrograph from this sample is presented in Figure IV.2.14. The disappearance of the large, thin hexagonal crystals with numerous small holes, is noteworthy. Also, the appearance of numerous dense spherical or hexagonal particles and the fiber-like γ-FeOOH particles is evident in Figure IV.2.14. Electron microdiffraction patterns obtained from the dense hexagonal/spherical particles confirmed them to be Fe_3O_4, while the patterns from the fiber-like particles showed γ-FeOOH structure in different orientations. The X-ray diffraction pattern exhibited the XRD profiles indicating a mixture of γ-FeOOH and Fe_3O_4. The XRD and microdiffraction data are in agreement and compliment each other.

IV.2.4.f. L6 Sample

This sample was withdrawn at a pH of 6.0 after 87 minutes of oxidation. A typical electron micrograph obtained from this sample is presented in Figure IV.2.15. Notable features are the development of long, fiber-like particles. Also, small dense or thin hexagonal particles can be seen. X-ray diffraction analysis showed only the presence of γ-FeOOH and trace amounts of α-FeOOH. Electron microdiffraction results indicate that the fiber-like particles are γ-FeOOH and the dense hexagonal particles are of Fe_3O_4 structure.

IV.2.4.g. L7 Sample

This sample was withdrawn at a pH of about 4 after 107 minutes of oxidation. For this sample, only fiber-type particles of γ-FeOOH could be observed; the absence of small dense hexagonal particles is noteworthy. A typical electron micrograph obtained from this sample (Figure IV.2.16) showed the presence of γ-FeOOH fibers. The X-ray diffraction pattern and electron diffraction patterns both confirm the presence of γ-FeOOH phase.

IV.2.4.h. L8 Sample

A typical electron micrograph obtained from this sample (Figure IV.2.17) shows that only fiber particles of γ-FeOOH are present. This sample does not show any other particle morphology such as hexagonal or spherical particles. X-ray diffraction results (Figure IV.2.18) confirm that this sample contains γ-FeOOH and only trace amounts of α-FeOOH.

IV.2.5. DISCUSSION

In the present investigation, the electron microdiffraction technique was utilized to follow the crystal structure and shape morphology at various stages of Fe^{2+} oxidation to produce γ-FeOOH.

Iron was present as Fe^{2+} at the beginning of the oxidation; the state of iron in the end product is γ-FeOOH. Therefore, several samples were withdrawn at various stages of oxidation. Initially, the pH of the suspension was about 8.2, and up to about 37 minutes, it remains almost constant (Figure IV.2.1). The pH of the suspension suddenly dropped to about 7.0 after 37 minutes, and after this sudden fall there is a gradual decline to pH 6 and then again there is a sudden drop in pH after 87 minutes, and after this rapid fall in pH, the pH remains almost constant at about 4.

Electron microscopy data provide information to define a pattern in the structural and morphological changes with the Fe^{2+} oxidation. As the iron oxyhydroxide samples are extremely susceptible to air-oxidation, caution must be exercised in handling these samples. The withdrawn samples were carefully washed and dried under nitrogen and the specimens for electron microscopy were prepared in a glovebox. The TEM specimens were stored in vacuum until their insertion into the microscope. Hence, all the samples investigated in this electron microscopy study were not exposed to air except for less than a minute while placing the TEM grid on the specimen holder and inserting the holder into the microscope.

Electron microscopy data obtained from these samples yield a definitive pattern in structural and shape morphologies and pictures representing the pattern of changes in particle morphology for samples L1 through L8 are presented in Figure

IV.2.19. Sample L1, withdrawn before oxygen flow was initiated, exhibited regions of dense, elongated particles and regions of shapeless thin regions. Reliable X-ray diffraction data were not obtained for this sample because the color changed from white to brown immediately upon placing the sample in the X-ray diffractometer, indicating rapid aerial oxidation. The sample L2, which was withdrawn after 13 minutes, did not exhibit a significant difference in morphology from L1. The elongated dense curly particles, several spherical particles and shapeless thin regions were evident in both these samples. Using the electron microdiffraction technique, $Fe(OH)_2$ particles were identified from regions as small as 5 nm. Both the spherical and the shapeless, transparent particles are $Fe(OH)_2$. Thus, iron hydroxide ($Fe(OH)_2$) is present in two morphological shapes. The microdiffraction technique is a useful tool in obtaining crystallographic information from these small 5 nm or 2 nm particles.

The electron micrographs obtained from sample L3 clearly indicates a change in the shape from that of L2. Large thin hexagonal crystals were formed and, surprisingly, these hexagonal crystals contained numerous small holes. These holes were in the range of 2-3 nm; however, a few atypical regions exhibited holes as large as 12-14 nm. Both X-ray diffraction and electron diffraction data show that the large, thin hexagonal particles are GR-II. This sample consists predominantly of large thin hexagonal crystals; very few, if any, needle-type particles are present. The X-ray diffraction pattern from this sample confirm the structure to be GR-II_{hcp}. Sample L4 exhibited quite similar features as sample L3, but the presence of dense Fe_3O_4 hexagonal particles was evident in sample L4. However, the number of large hexagonal crystals exceeds that of the small, dense hexagonal particles for sample L4.

A significant change in morphology was noticed for sample L5. The large thin hexagonal crystals, which are GR-II, are not present and more needle-type γ-FeOOH particles are evident. Small, dense hexagonal Fe_3O_4 particles are present; however, the number of such particles in sample L6 is much less than in L5, and the needles are present in greater number. For samples L7 and L8, the formation of needle-type γ-FeOOH appears to be complete, and no dense, small hexagonal Fe_3O_4 particles can be observed.

There was a transformation of GR-II to Fe_3O_4 during the first rapid change in pH. An important observation was that Fe_3O_4 was found only in L4 and L5 samples and not in the final product. Hence, Fe_3O_4 formed during the pH change from 8 to 7.0 must subsequently be transformed to γ-FeOOH either by reforming GR-II or by directly transforming to γ-FeOOH. As shown by the pictorial sequence in Figure IV.2.20, the transformation pathway is from $Fe(OH)_2$ to a Green Rust complex, then to a mixture of Green Rust and Fe_3O_4 to γ-FeOOH. As Fe_3O_4 is formed at a pH of 6.5 (sample L5) the ratio of Fe^{3+} to Fe^{2+} in solid phase is about 2:1. The remaining Fe^{2+} ions are oxidized with a slow decrease in pH and when all the Fe^{2+} ions present in the solid phase were transformed to Fe^{3+} ions, again a sudden drop in pH from about 6.5 to 4.0 was noticed. The final product is γ-FeOOH.

IV.2.6. ACKNOWLEDGMENT

This work was supported by the DOE contract #DE-AC22-91PC90056 and the Commonwealth of Kentucky. The microscope facilities offered by the Materials Characterization Facilities, University of Kentucky is gratefully acknowledged.

IV.2.7. REFERENCES

IV.2.1. Misawa, T.; Kyuno, T.; Suétaka, W.; Shimodaira, S. *Corros. Sci.*, **1971**, *11*, 35.

IV.2.2. Evans, U. R. "The Corrosion and Oxidation of Metals", 1st Suppl. Vol., p 185, Arnold, London, 1968.

IV.2.3. Keller, P. *Wekstoffe Korros.*, **1967**, *18*, 865.

IV.2.4. Molgaard, J., 5th International Congress on Metallic Corrosion, Tokyo, Japan, 1972.

IV.2.5. Nagayama, M.; Cohen, M. *J. Electrochem. Soc.*, **1962**, *109*, 781.

IV.2.6. Bernal, J. D.; Dasgupta, D. A.; Mackay, A. L. *Clay Miner. Bull.*, **1959**, *4*, 15.

IV.2.7. Mackay, A. L. "Reactivity of Solids", (J. H. De Boer, et al., eds.), Elsevier, Amsterdam, p 571, 1961.

IV.2.8. Takada, T. *Bull. Inst. Chem. Res.*, Kyoto University, **1969**, *47*, 298.

IV.2.9. Kiyama, M. *Bull. Inst. Chem. Res.*, Kyoto University, **1969**, *47*, 607.

IV.2.10. Kiyama, M.; Takada, T. *Bull. Chem. Soc. Japan*, **1972**, *45*, 1923.

IV.2.11. Misawa, T.; Hashimoto, K.; Shimodaira, S. *Corros. Sci.*, **1974**, *14*, 131.

IV.2.12. Keller, G., Thesis, Bern, 1948.

IV.2.13. Feitknecht, W.; Keller, G. *Z. Anorg. Chem.*, **1950**, *262*, 61.

IV.2.14. Olowe, A. A.; Pauron, B.; Genin, J. M. R. *Corros. Sci.*, **1991**, *32*, 985.

Table IV.2.1

Sample Identifications and Time of Withdrawal

Sample ID	Time of Withdrawal after the NaOH Addition (min.)	pH at the time of Withdrawal	$(Fe^{2+}/Fe^{2+}+Fe^{3+})$
L1	0	8.22	1.00
L2	13	8.20	0.91
L3	37	8.25	0.70
L4	48	6.75	0.59
L5	67	6.50	0.41
L6	87	6.25	0.21
L7	107	4.15	0.15
L8	150	3.80	0.14

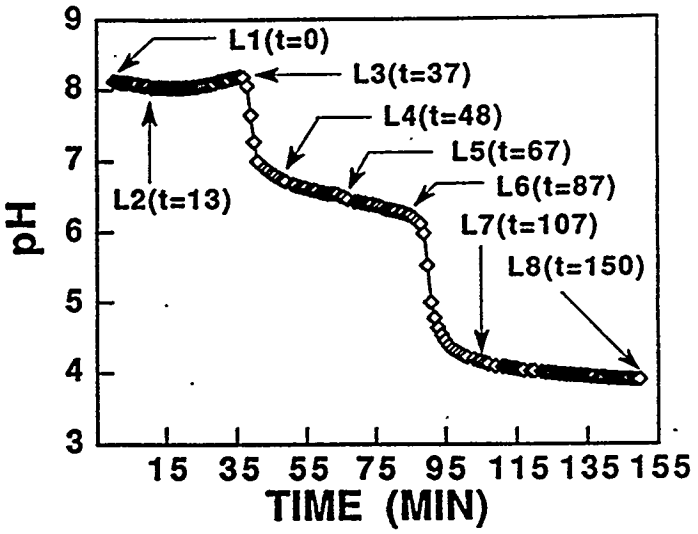

Figure IV.2.1. Variation in pH of the suspension with time. The samples L1 through L8 were withdrawn at several stages in this curve. The time the samples were taken has been mentioned within parenthesis after the sample number.

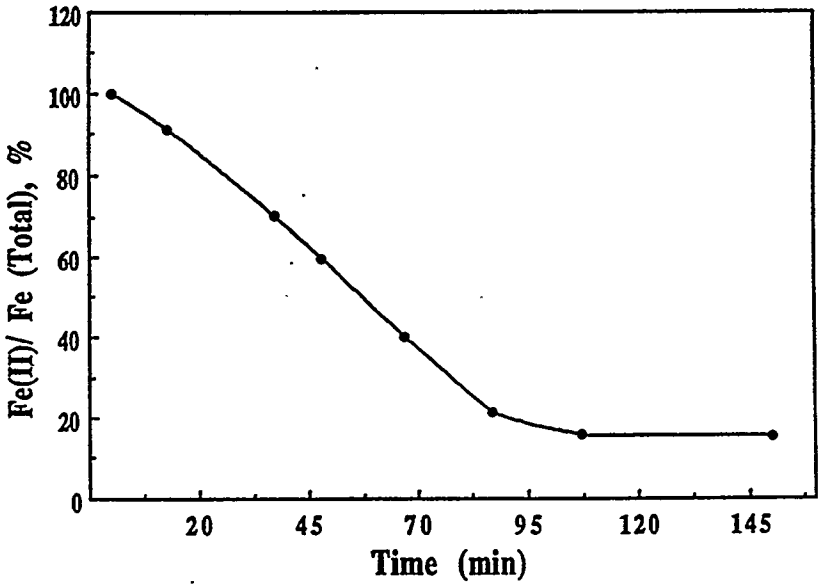

Figure IV.2.2. Estimation of concentration of Fe^{2+} and Fe^{3+} with time.

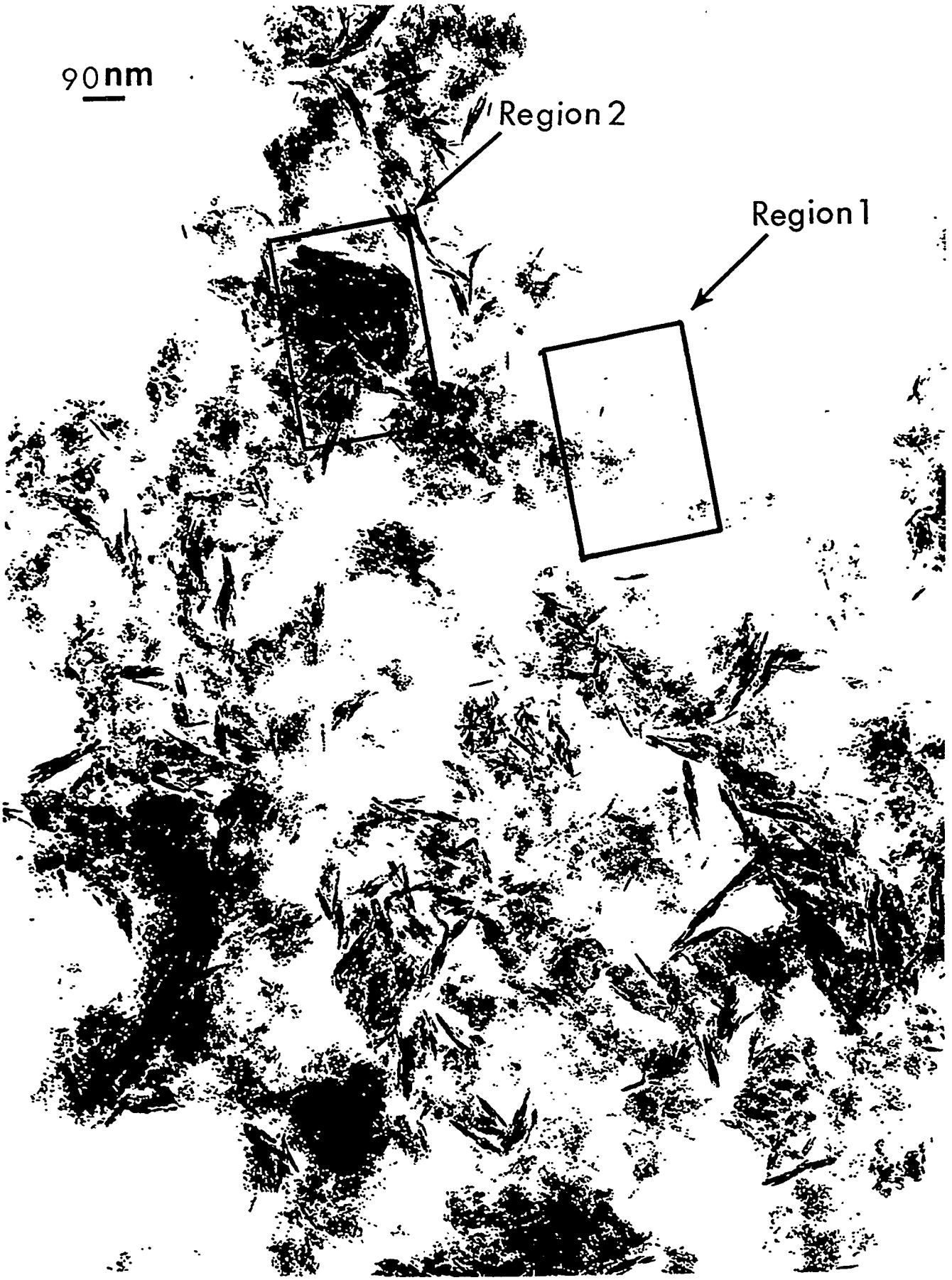

Figure IV.2.3. A typical electron micrograph obtained from the L1 sample. The presence of shapeless thin regions (region 1) and dense elongated curly particles (region 2) can be seen.

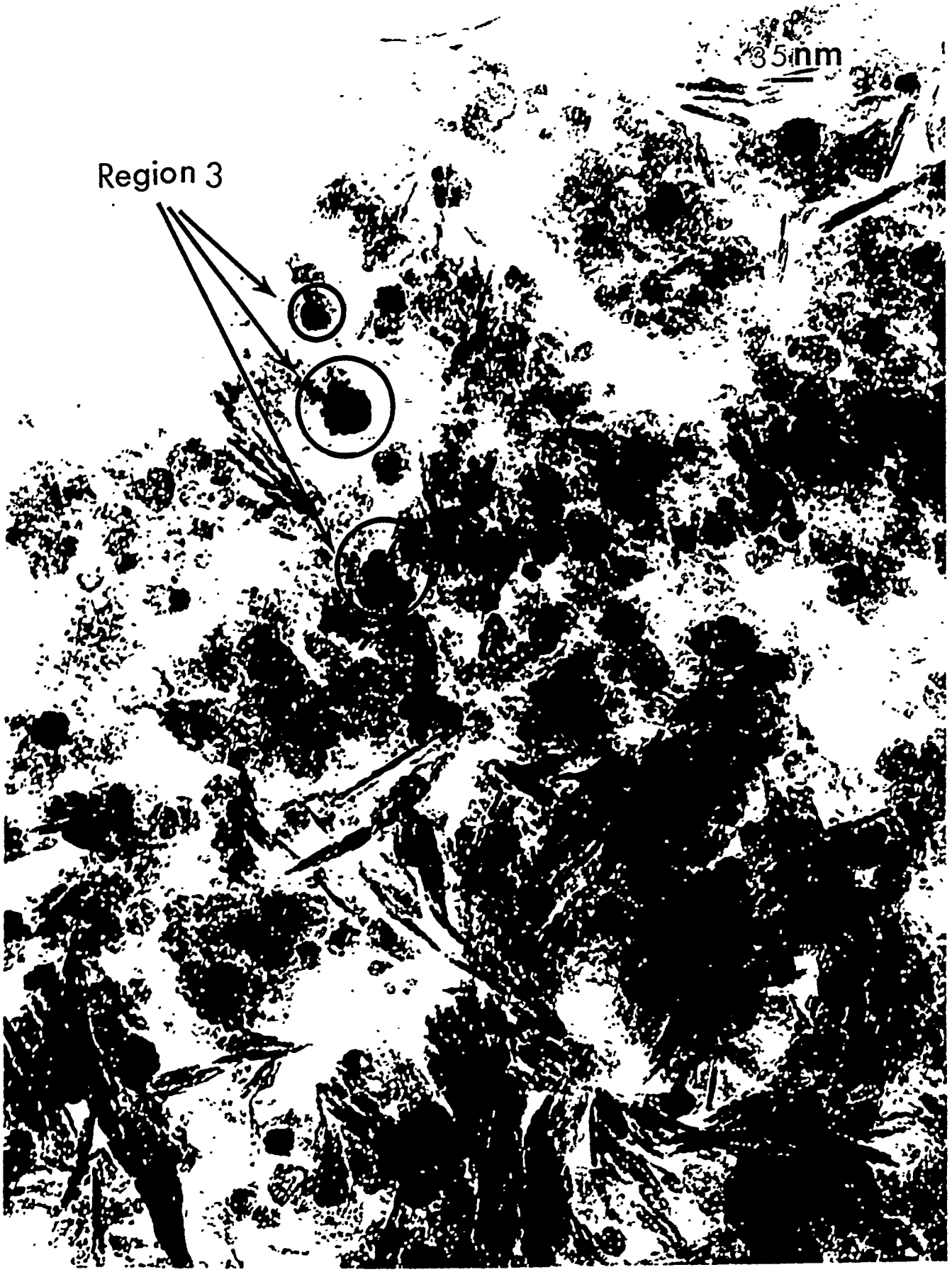

Figure IV.2.4. An electron micrograph obtained from the L1 sample. The presence of spherical particles (region 3) in addition to the features mentioned in Figure 3 can be seen.

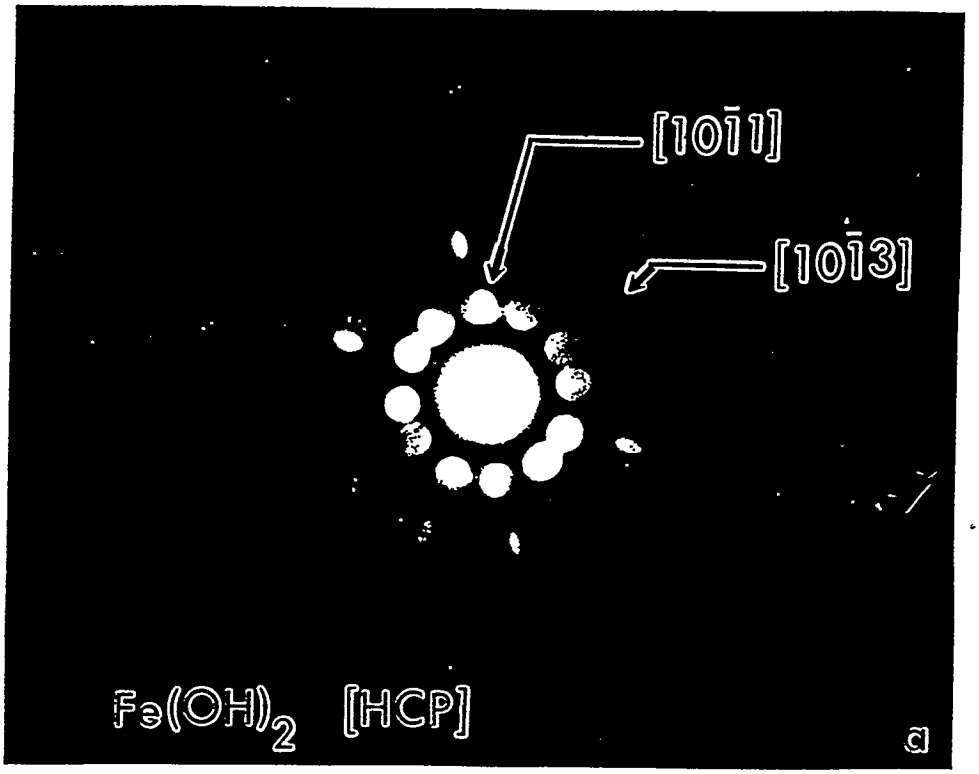

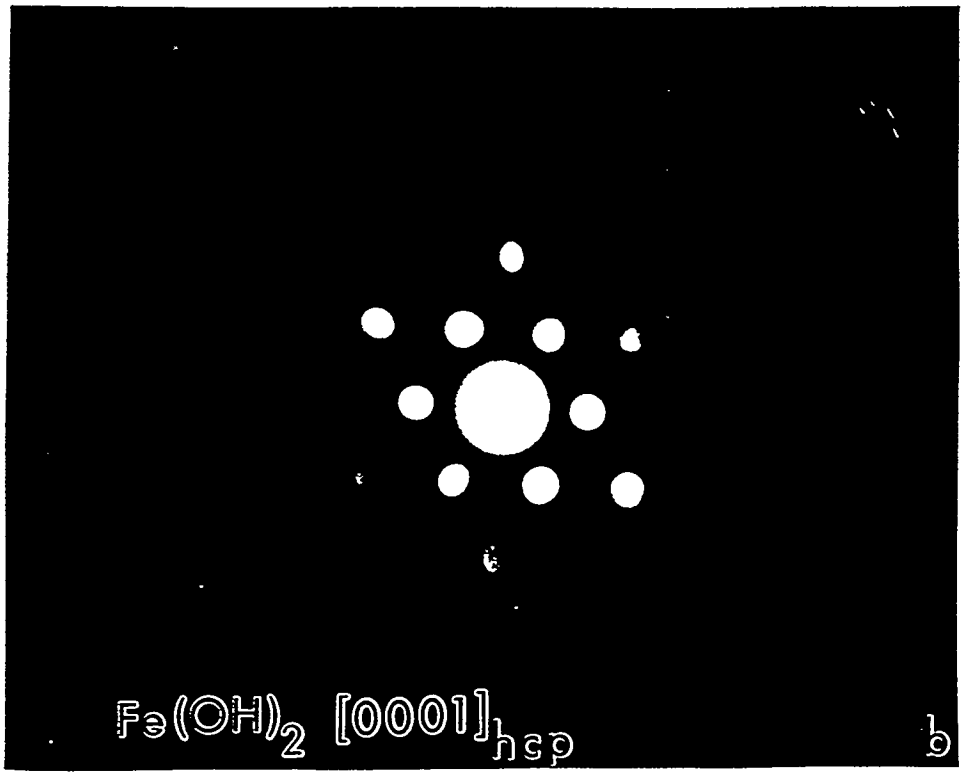

Figure IV.2.5. Electron microdiffraction patterns obtained from the sample L1 using a 5 nm electron probe: (a) from a thin shapeless region; the 1st and 2nd rings correspond to [101] and [103] planes of $Fe(OH)_2$ phase (hcp), and (b) from the spherical $Fe(OH)_2$ particle, which is in $[100]_{hcp}$ orientation.

Figure IV.2.6. An electron micrograph obtained from the L2 sample withdrawn after 13 minutes of oxidation. The morphological features are quite similar to those for sample L1. (a) From a most typical region, and (b) several individual dense spherical particles. [Inset] Microdiffraction patterns from the $Fe(OH)_2$ particles.

Figure IV.2.7. An electron micrograph obtained from sample L3, wherein thin hexagonal crystals with small holes can be seen. The size of these holes ranges from 2.5 to 3 nm.

Figure IV.2.8. An electron micrograph for sample L3, highlighting a region containing larger holes (12-14 nm in size).

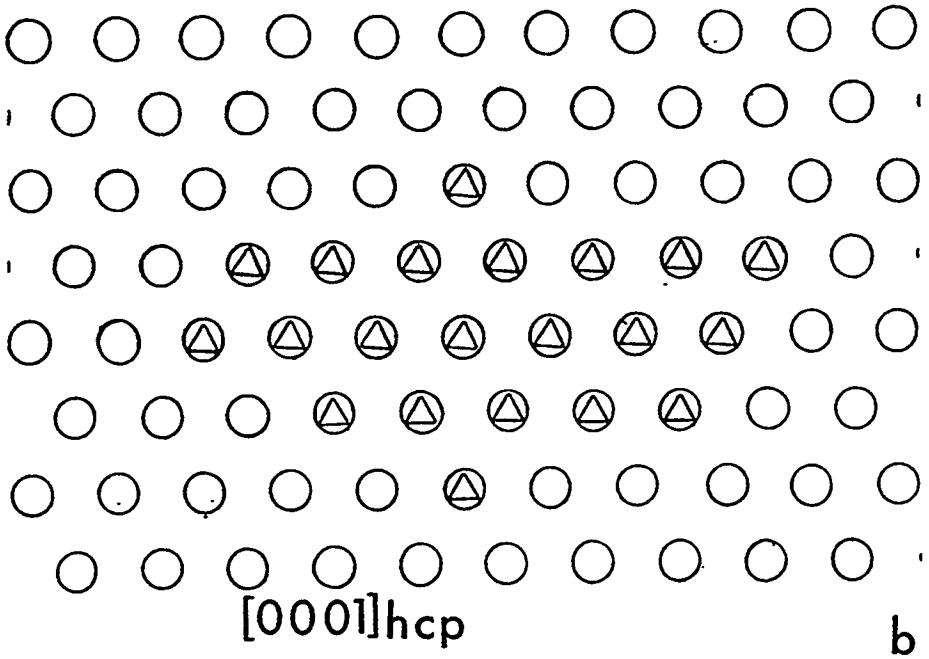

Figure IV.2.9. (a) Electron microdiffraction pattern obtained from a large hexagonal thin crystal (Sample L3). The crystal is in $[0001]_{hcp}$ orientation. (b) Corresponding solution (△) observed reflections, and (○) theoretically generated reflections.

Figure IV.2.10. A region indicating well formed γ-FeOOH needle-type particles in addition to the formation of the hexagonal crystals for sample L3 can be seen.

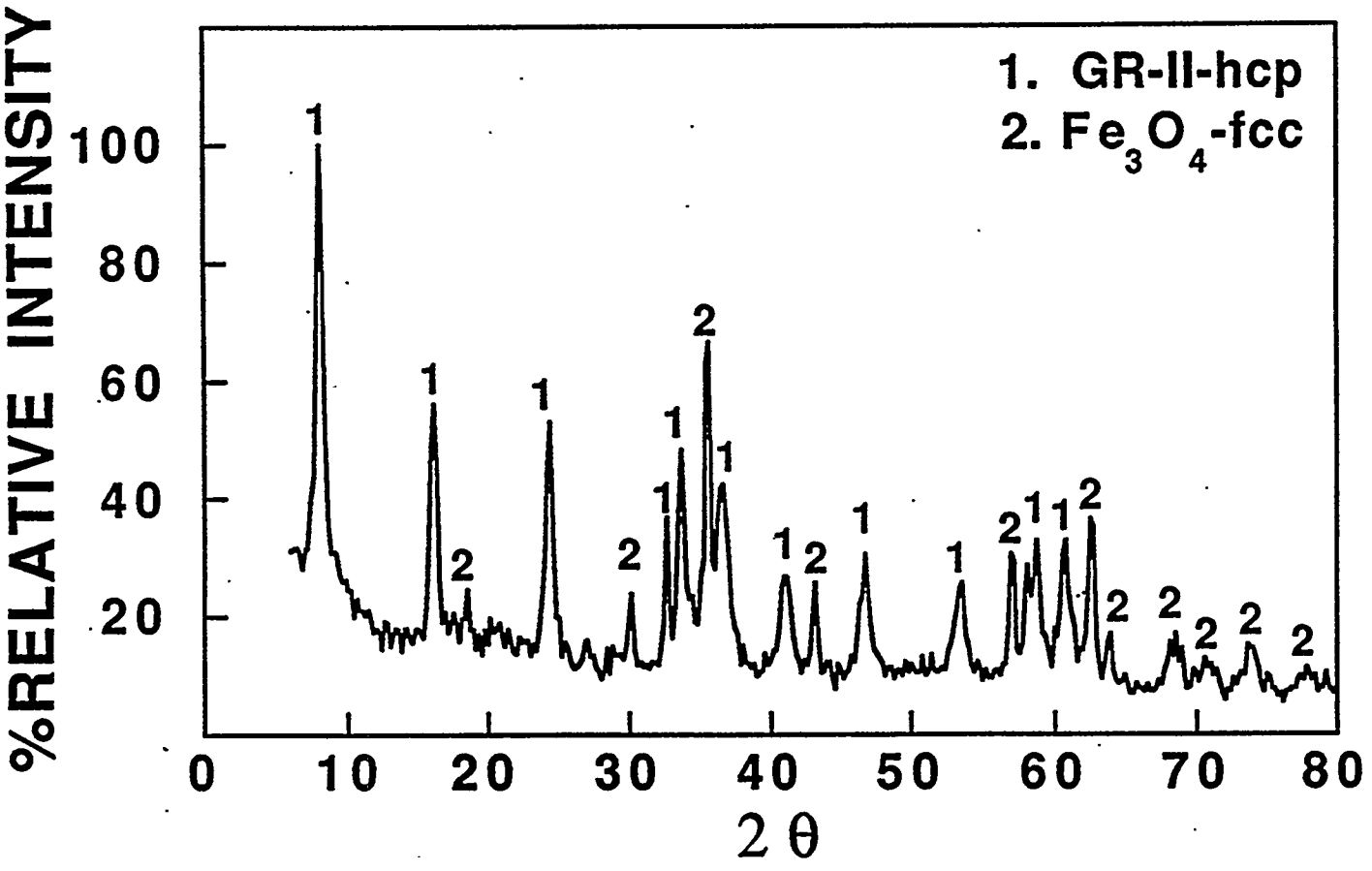

Figure IV.2.11. X-ray diffraction pattern from the sample L4. The peaks corresponding to GR-II and Fe_3O_4 phases are indicated.

Figure IV.2.12. A representative electron micrograph from sample L4. Note the appearance of dense hexagonal Fe_3O_4 particles.

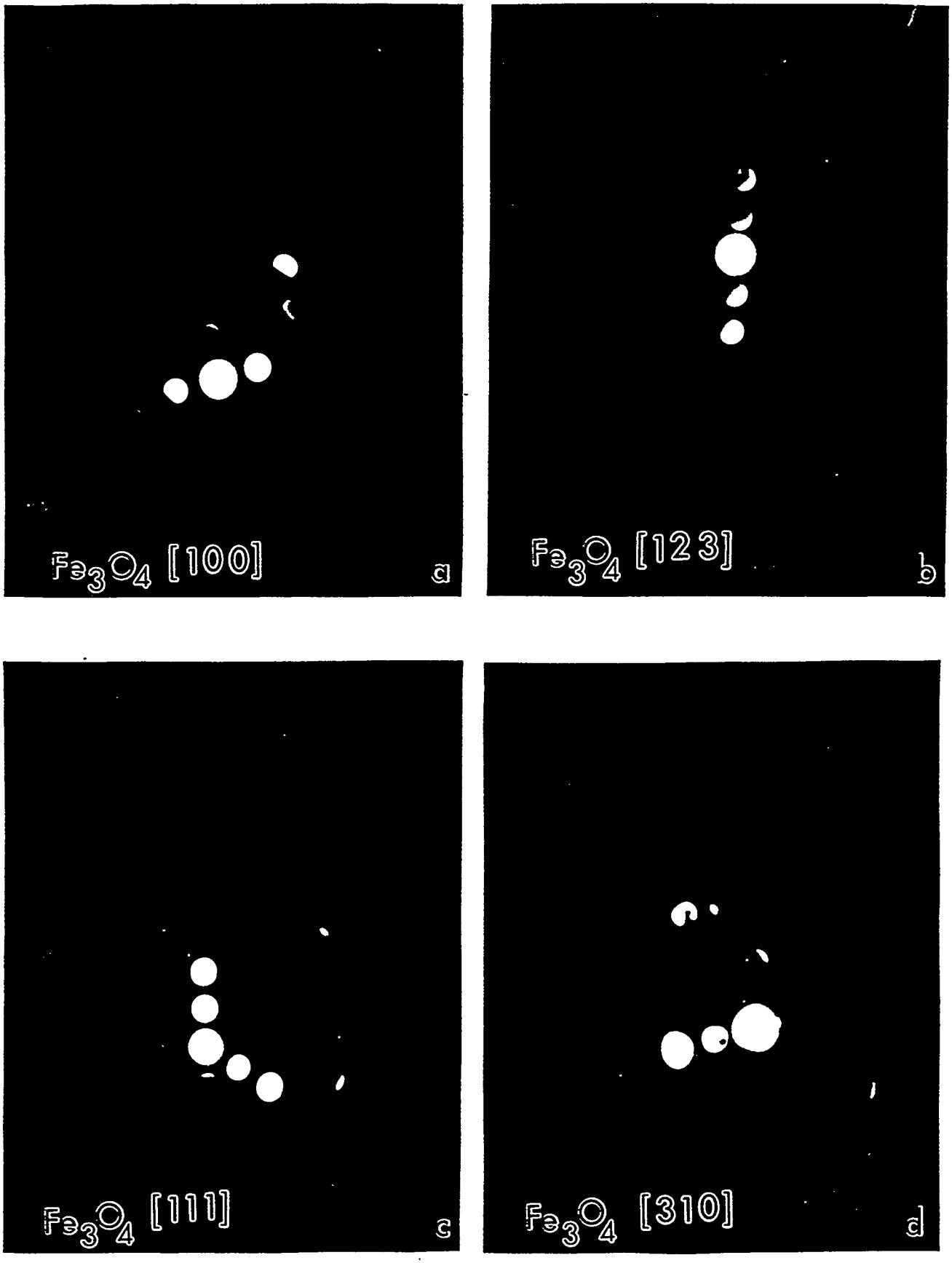

Figure IV.2.13. Four most densely populated electron microdiffraction patterns obtained from several dense hexagonal particles of sample L4 as indicated by arrows in Figure 12. All these patterns yielded $(Fe_3O_4)_{fcc}$ orientations. (a) [100], (b) [123], (c) [111], and (d) [310].

Figure IV.2.14. A typical electron micrograph from the L5 sample. Note the disappearance of large, thin hexagonal crystals with holes and the appearance of more number of dense spherical or hexagonal particles as well as the fiber-like γ-FeOOH particles.

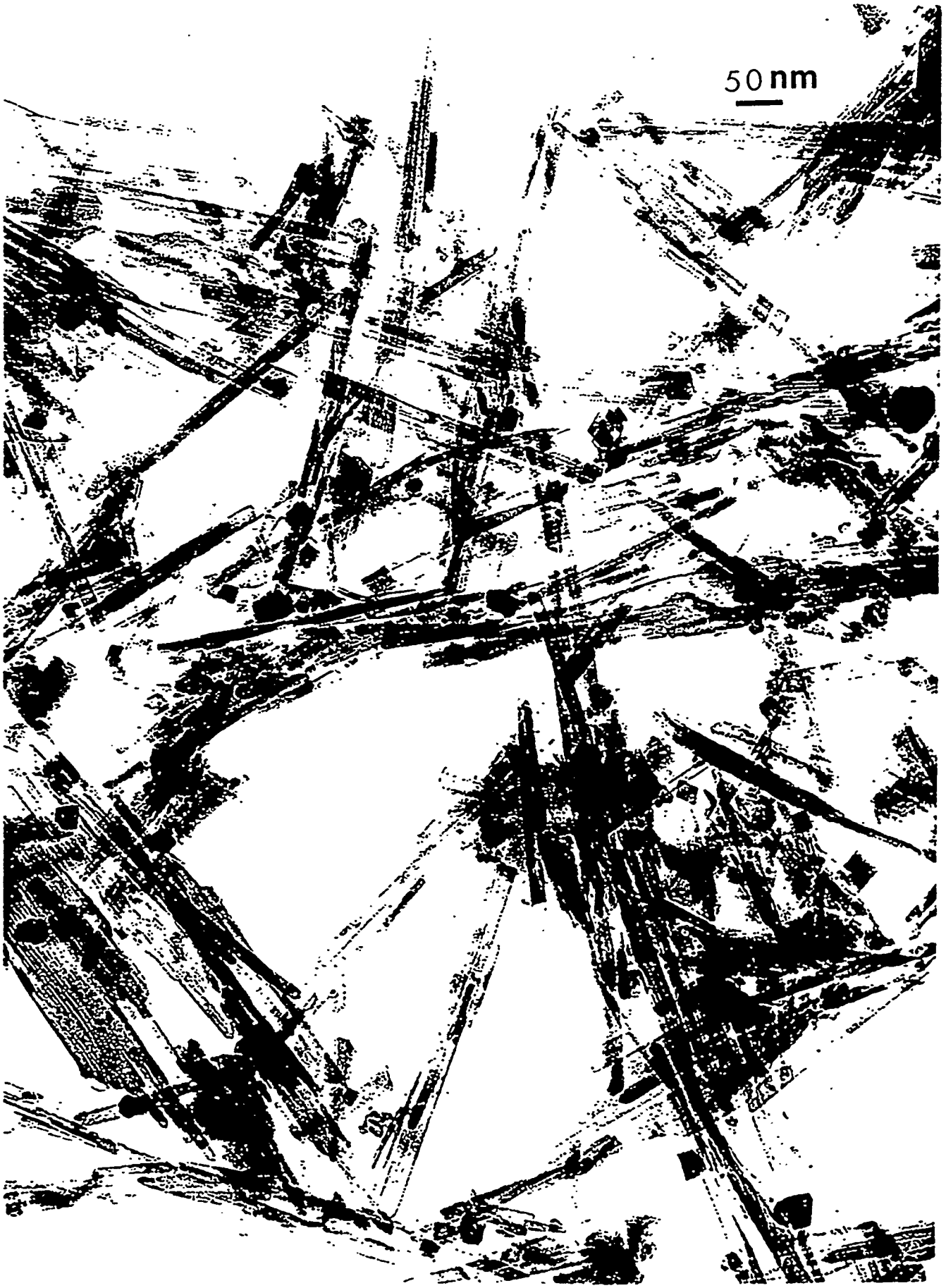

Figure IV.2.15. An electron micrograph from sample L6. Long fibers of γ-FeOOH can be seen; also, note the presence of a reduced number of dense small hexagonal Fe_3O_4 particles.

Figure IV.2.16. A typical electron micrograph from Sample L7. Note the presence of only fiber-like particles. [Inset] Electron microdiffraction pattern obtained from one of the thin fiber γ-FeOOH particle is in [142] orientation.

Figure IV.2.17. Electron micrograph from sample L8.

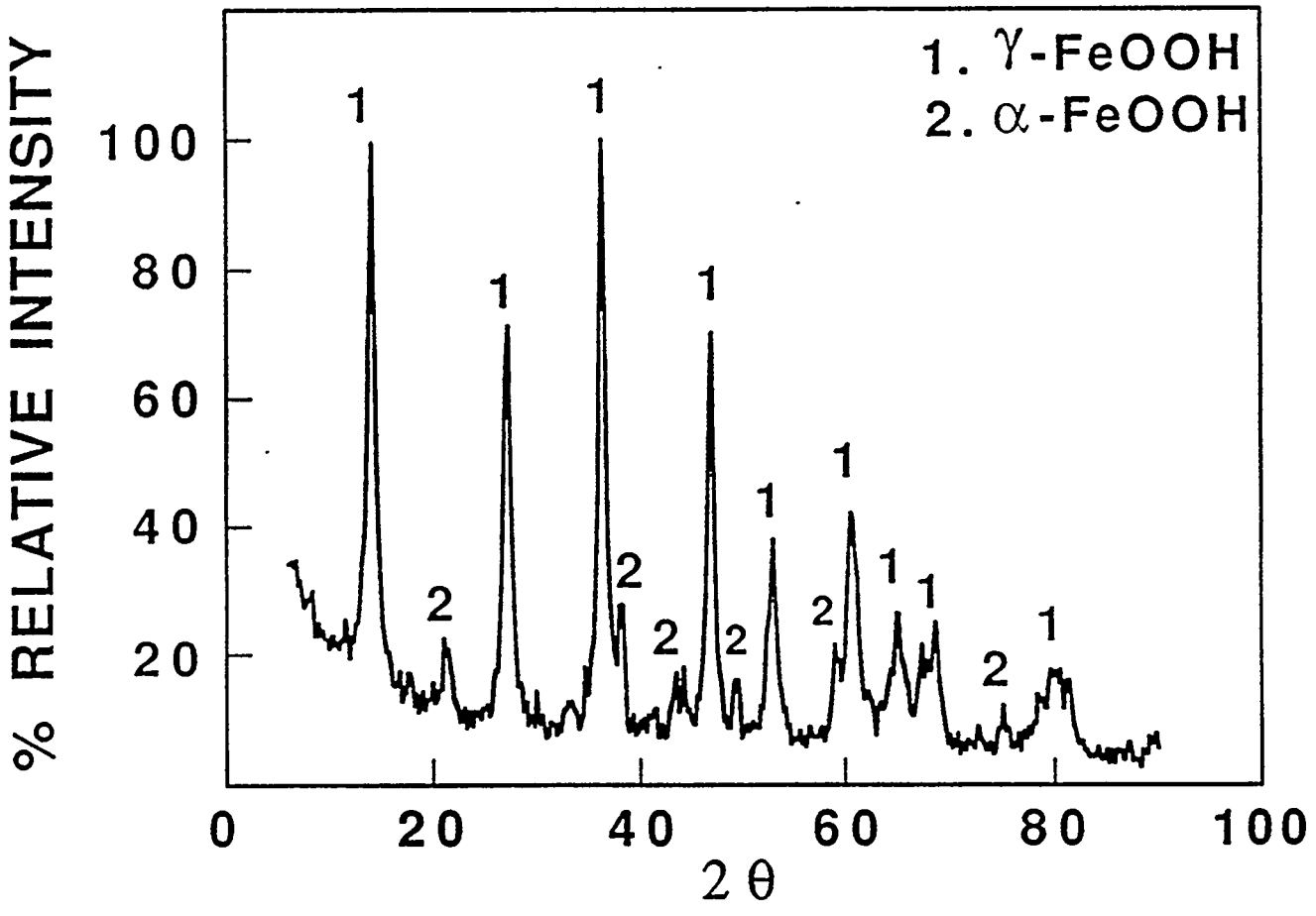

Figure IV.2.18. X-ray diffraction pattern obtained from sample L8 showing γ-FeOOH phase and trace amounts of α-FeOOH.

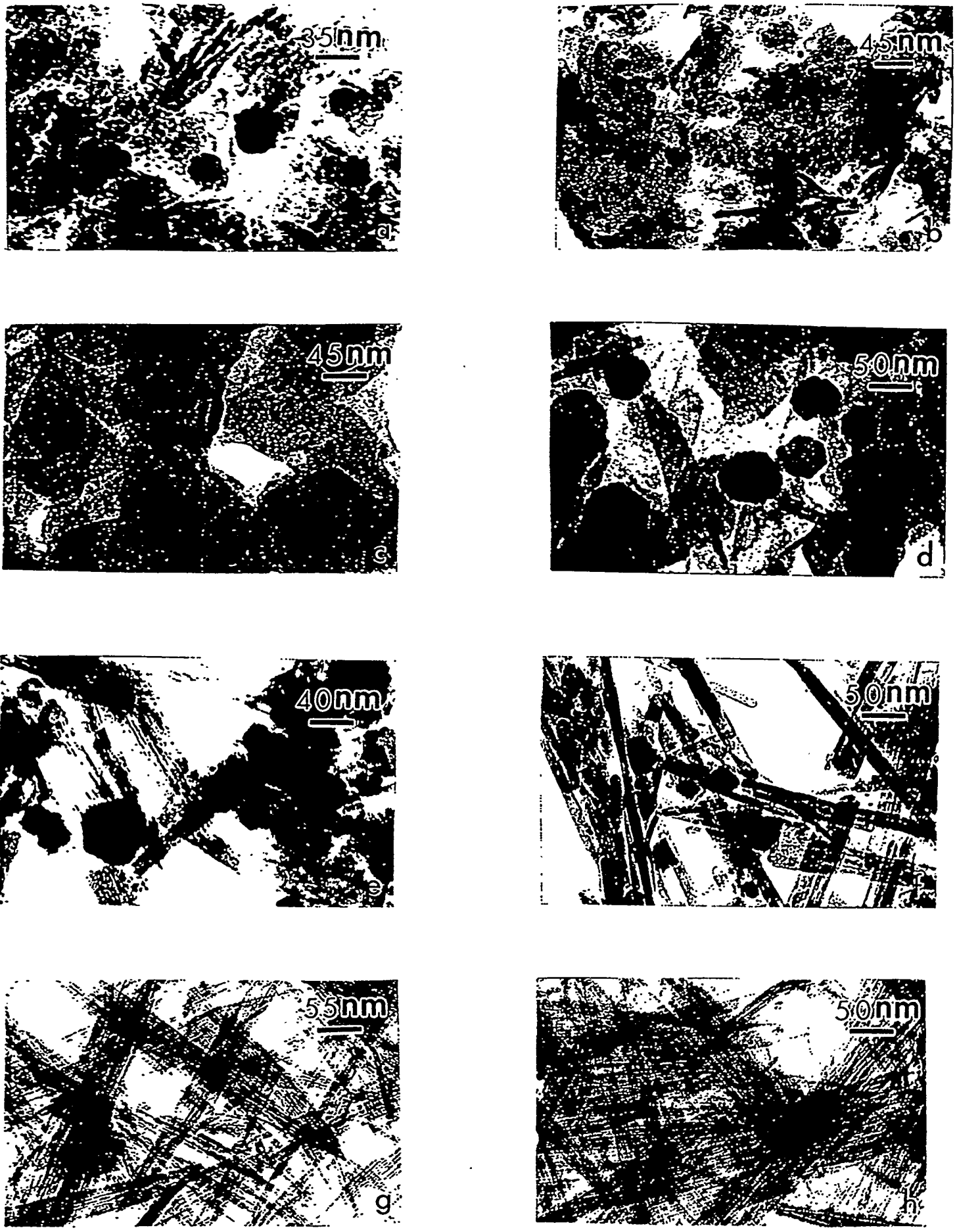

Figure IV.2.19. A schematic representation of a pattern of changes in shape/structure morphology from samples L1 to L8.

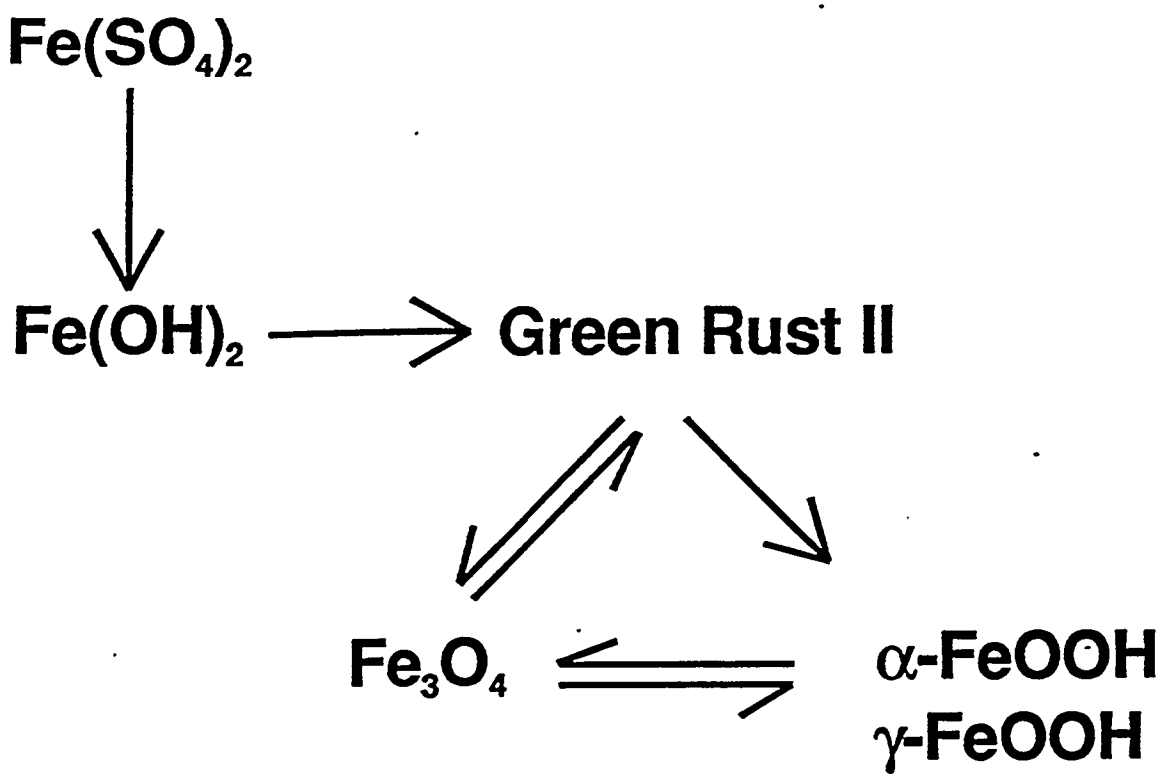

Figure IV.2.20. A pictoral sequence representing the oxidation pathway from $Fe(OH)_2$ to γ-FeOOH.